

# **■** Donor–Acceptor Systems

# Evaluation of Pd→B Interactions in Diphosphinoborane Complexes and Impact on Inner-Sphere Reductive Elimination

Florian Ritter, Lukas John, Tobias Schindler, Julian P. Schroers, Simon Teeuwen, and Michael E. Tauchert\*<sup>[a]</sup>

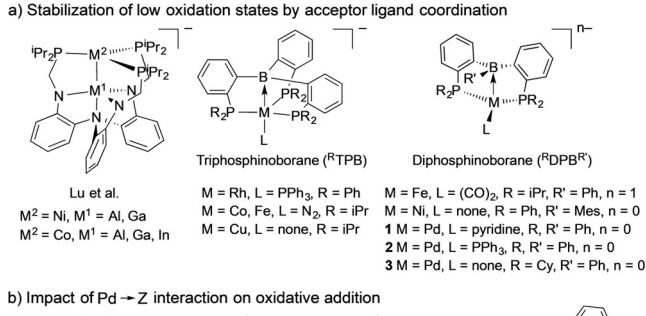
**Abstract:** The dative  $Pd \rightarrow B$  interaction in a series of  $^RDPB^{R'}$   $Pd^0$  and  $Pd^{II}$  complexes  $(^RDPB^{R'} = (o - PR_2C_6H_4)_2BR'$ , diphosphinoborane) was analyzed using XRD,  $^{11}B$  NMR spectroscopy and NBO/NLMO calculations. The borane acceptor discriminates between the oxidation state  $Pd^{II}$  and  $Pd^0$ , stabilizing

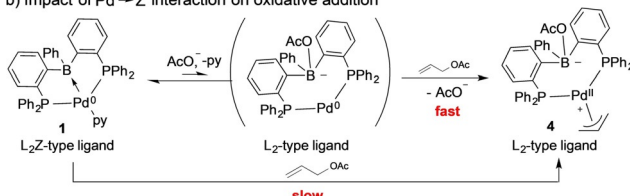
the latter. Reaction of lithium amides with  $[(^RDPB^R)Pd^{II}(4-NO_2C_6H_4)I]$  chemoselectively yields the C–N coupling product. DFT modelling indicates no significant impact of  $Pd^{II} \rightarrow B$  coordination on the inner-sphere reductive elimination rate.

# Introduction

Z-type acceptor ligands have attracted considerable attention over the past decade.<sup>[1]</sup> Their coordination to transition metals grants access to complexes with unusual coordination geometries<sup>[2]</sup> and electronic properties by formation of dative  $M \rightarrow Z$ bonds. Group 13 acceptor ligands, with a special focus on boranes, have been particularly well studied. M→Z bonds can stabilize low oxidation states at the coordinated transition metal.[3] Thus, facile access to complexes featuring transition metals with formally negative oxidations states is realized (Figure 1 a). [4] This stabilization of low oxidation states appears to inhibit oxidative addition reactions.[3b,e,5] However, we demonstrated that this obstacle can be overcome for complex 1 by addition of catalytic amounts of acetate, which competes with Pd<sup>0</sup> for the free coordination site at the borane, thus reversibly breaking the Pd<sup>0</sup>→B interaction (Figure 1b).<sup>[3b]</sup> This concept allowed for the application of 1 in catalytic allylic amination, and most recently of 2 in the catalytic hydro-/deutero-dechlorination of aryl chlorides.[3e] Alternatively, bifunctional substrate activation across the  $M{\to}Z$  interaction has been described. [3a,6] The aptitude of hydride, [7] halide [8] and carbon group [9] migration between the Z-type ligand and the coordinated transition metal has initiated further applications. Catalytic processes have concentrated on transformations in which the catalyst is not required to change its oxidation state quickly, but rather profits from an electronic fine-tuning by electron-withdrawing Z-ligand coordination. Successful applications include  $CO_2$  hydrogenation and hydrosilylation, successful applications include  $CO_2$  hydrogenation and hydrosilylation, successful applications include  $CO_2$  hydrogenation and hydrosilylation, successful applications with hidrogenization and alkyne hydroamination. Michaelis used the heterobimetallic  $Ti^{IV}/Pd^{II}$  complex (Figure 1 c), developed by Nagashima, for allylic amination of allyl chlorides with hindered secondary amines. Successful applications include  $CO_2$  hydrogenization and hydrogenizations include  $CO_2$  hydrogenizations include  $CO_2$  hydrogenization applications include  $CO_2$  hydrogenizations include  $CO_2$  hydrogenizati

Combined experimental and computational investigations indicated a rate enhancement of  $10^{3-}$ – $10^{5}$  of the outer-sphere reductive C–N bond elimination, due to the electron-withdraw-





c) Impact of Pd → Z interaction on reductive elimination

**Figure 1.**  $M \rightarrow Z$  interaction: stabilization of low oxidation states and impact on oxidative addition and reductive elimination.

Supporting information and the ORCID identification number(s) for the author(s) of this article can be found under: https://doi.org/10.1002/chem.202001189.

© 2020 The Authors. Published by Wiley-VCH GmbH. This is an open access article under the terms of the Creative Commons Attribution License, which permits use, distribution and reproduction in any medium, provided the oriainal work is properly cited.

<sup>[</sup>a] F. Ritter, Dr. L. John, Dr. T. Schindler, J. P. Schroers, S. Teeuwen, Dr. M. E. Tauchert Institute of Inorganic Chemistry, RWTH Aachen University Landoltweg 1A, 52074 Aachen (Germany) E-mail: Michael.Tauchert@ac.rwth-aachen.de



ing  $Pd^{II} \rightarrow Ti^{IV}$  interaction. [5b,17] This result agrees with previous investigations performed with Pd  $\eta^3$ -allyl and Ni  $\eta^3$ -allyl complexes, which showed favored reductive outer-sphere reductive elimination in the presence of less electron-donating spectator ligands. [18]

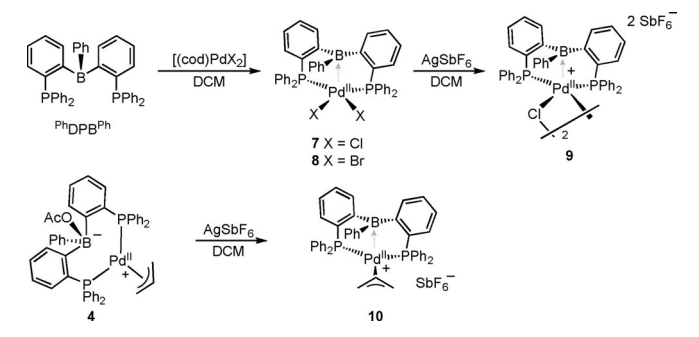
We speculated that the electron-withdrawing properties of the borane functionality in diphosphinoborane (DPB) ligands enhances the rate of inner-sphere reductive elimination from Pd complexes due to 1) overall reduced electron density at the Pd $^{\parallel}$  center and 2) increasing of the Pd $\rightarrow$ B interaction strength during reductive elimination. We determine how the oxidation state of Pd and co-ligands affect the strength of the Pd $\rightarrow$ B interaction in DPB complexes. NBO/NLMO calculations and solid-state structures are used to assess the strength of Pd $\rightarrow$ B interactions. The value of the  $^{11}$ B NMR chemical shift as a probe is discussed. The reductive elimination of N,N-dimethyl-4-nitroaniline from [( $^{Ph}$ DPB $^{Ph}$ )Pd $^{\parallel}$ (4-NO $_2$ -C $_6$ H $_4$ )NMe $_2$ ] (5) was studied and modelled with DFT calculations to investigate the assumed influence of the borane acceptor.

# **Results and Discussion**

# Syntheses and reactivity of [(DPB)Pd] complexes

A series of  $[(^{Ph}DPB^{Ph})Pd^{II}]$  complexes was synthesized to examine a possible correlation between the nature of ligands at Pd and the strength of the  $Pd^{II} \rightarrow B$  interaction (Scheme 1).

Complex  $[(^{Ph}DPB^{Ph})Pd^{II}Cl_2]$  (7) was produced by reaction of  $^{Ph}DPB^{Ph}$  ligand with  $[(cod)PdCl_2]$  in DCM and was isolated in 74% yield (Scheme 1). Single crystals were grown from  $CH_2Cl_2$ / benzene and analyzed by X-ray diffraction (Figure 2). A typical square-pyramidal coordination around the palladium was observed around the Pd<sup>II</sup> center. The chloride ligands are located in *cis*-configuration at the basal position, and the borane adopts the apical position. The Pd,B distance of 2.762(3) Å is shorter than the sum of the van der Waals radii (3.28 Å), 19 but elongated compared to the sum of the covalent radii (2.23 Å). A long Pd,C51 distance of 3.405(3) Å seems to rule out a  $\eta^2$ -(B,C) type coordination to the Pd<sup>II</sup> center. A slightly in-



**Scheme 1.** Synthesis of [(PhDPBPh)Pdll] complexes.

creased pyramidalization at the boron atom is observed ( $\Sigma B_a = 355.4^{\circ}$ ) compared to complex [( $^{\text{IP}}\text{TDPB}^{\text{Ph}}$ )PdCl<sub>2</sub>] ( $\Sigma B_a = 359.9^{\circ}$ ).[21]

The ligand backbone is twisted (dihedral angle C62-C61-C71-C72: 35.6(3)°) to allow for a P-Pd-P angle of 95.49(3)°. This twist renders the two phosphine groups diastereotopic. The  $^{31}\text{P}$  NMR spectrum of **7** in CD<sub>2</sub>Cl<sub>2</sub> displays two broad resonances of equal integral at  $\delta=39.0$  and 48.2 ppm. A series of  $^{31}\text{P}$  VT NMR spectra was recorded (Figure 3), covering a temperature range from -29.8 to  $35.1\,^{\circ}\text{C}$ . The two singlet resonances coalesced into a single resonance ( $\delta=48.2$  ppm) at elevated temperatures. The rate constants of the dynamic process were determined by line-shape analysis using Bruker's TopSpin software. An Arrhenius plot analysis gave an activation energy of

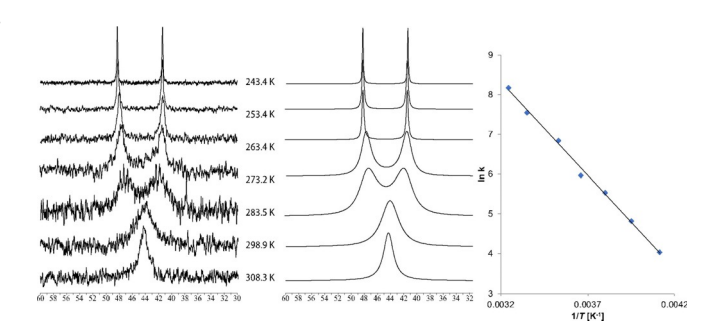


**Figure 3.**  $^{31}P$  VT NMR analysis of **7** in CD<sub>2</sub>Cl<sub>2</sub>. Left: recorded  $^{31}P$  NMR spectra. Middle: simulated  $^{31}P$  NMR spectra. Right: Arrhenius plot.

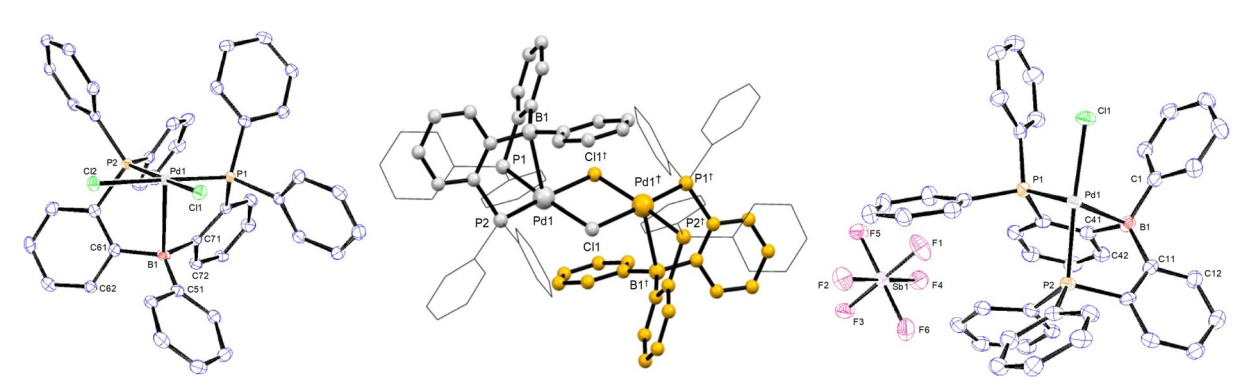


Figure 2. Left: thermal ellipsoid plot of the solid-state structure of 7 at the 50% probability level. Hydrogen atoms are omitted for clarity. Selected bond lengths (Å) and angles (°): Pd1–Cl1 = 2.3355(7), Pd1–Cl2 = 2.3628(7), Pd1–P1 = 2.2558(8), Pd1–P2 = 2.2932(8), Pd1–B1 = 2.762(3), Pd1–C51 = 3.405(3), P1-Pd1-P2 = 95.49(3), C51-B1-C61 = 118.3(3), C51-B1-C61 = 118.2(3), C71-B1-C61 = 118.8(3), [22] Middle: Ball and stick display of  $[(^{Ph}DPB^{Ph})PdCl]$ -dimer (9) generated by symmetry. Right: thermal ellipsoid plot of the asymmetric unit of 9 at the 50% probability level. Hydrogen atoms and crystal  $CH_2Cl_2$  are omitted for clarity. Selected bond lengths (Å) and angles (°): Pd1-Cl1 = 2.3781(11), Pd1-Cl1 = 2.3928(13), Pd1-P1 = 2.2638(13), Pd1-P2 = 2.3084(11), Pd1-B1 = 2.721(5), Pd1-C1 = 3.338(4), P1-Pd1-P2 = 95.38(5), C11-B1-C41 = 117.5(4), C1-B1-C11 = 119.4(4), C1-B1-C41 = 118.9(4).



 $E_a = 9.3 \pm 0.5 \text{ kcal mol}^{-1}$  with a pre-exponential factor of  $A = (14 \pm 7) \times 10^9$ .

We suggest that the observed dynamic process in the <sup>31</sup>P NMR spectrum of **7** is caused by an interconversion of **7** with its enantiomer *ent-***7** (Scheme 2).

Scheme 2. Proposed interconversion between 7 and *ent-*7 by twisting of the DPB ligand.

In order to accommodate for the small P-Pd-P angle of  $95.49(3)^{\circ}$ , the  $\sigma$ -symmetric <sup>Ph</sup>DPB<sup>Ph</sup> ligand is twisted. As a result, its B—Ph group points towards one of the two phosphine groups, rendering them chemically inequivalent. This assumption is in line with the observed two <sup>31</sup>P NMR resonances at low temperatures. Twisting of the C62-C61-C71-C72 dihedral angle converts **7** into its enantiomer *ent-***7**, presumably via a  $\sigma$ -symmetric transition in which the B—Ph group is orientated between the two chloro ligands.

Complex **8** was synthesized in the same fashion as **7** from [(cod)PdBr<sub>2</sub>] and was isolated in 67% yield. The <sup>31</sup>P NMR spectrum displays two broad resonances of equal intensity at  $\delta$  = 45.2 and 38.1 ppm (CD<sub>2</sub>Cl<sub>2</sub>), suggesting a similar dynamic process as in **7**. Due to the poor solubility of both **7** and **8**, no <sup>11</sup>B NMR spectra could be obtained.

Cationic complex [(PhDPBPh)PdICI]SbF<sub>6</sub> (9) was produced in 51% isolated yield by halide abstraction from 7 with AgSbF<sub>6</sub> (Scheme 1). Single crystals were grown from CH<sub>2</sub>Cl<sub>2</sub>/hexane and analyzed by X-ray diffraction (Figure 2). In the solid state a chloro-bridged dimer  $[(^{Ph}DPB^{Ph})Pd^{II}(\mu-CI)]_2(SbF_6)_2$  is observed with an inversion center between the two Pd<sup>II</sup> centers. Within the dimer, the Pd<sup>II</sup> center is coordinated in a square-pyramidal fashion with the borane located in the apical position. The Pd, B distance in complex 9 is 2.721(5) Å, which is slightly shorter than in  $[(^{Ph}DPB^{Ph})Pd^{\parallel}Cl_{2}]$  **7** (2.762(3) Å). However, pyramidalization of the borane is almost identical ( $\Sigma B_a = 355.8^{\circ}$ ). The absence of a relevant  $\eta^2(B,C){\to} Pd^{II}$  interaction is suggested by the long Pd1,C1 distance of 3.338(4) Å. The Pd,B distance and lack of significant pyramidalization at the borane suggest a weak Pd<sup>II</sup>→B interaction, which is in line with a broad resonance in the <sup>11</sup>B NMR spectrum at  $\delta$  = 65 ppm ( $\omega_{1/2}$  = 1900  $\pm$ 500 Hz).

The ligand backbone is twisted similarly to that in **7** (dihedral angle C42-C41-C11-C12 of  $33.5(5)^{\circ}$  (**9**) vs.  $35.6(3)^{\circ}$  in **7**), resulting in an almost parallel orientation of the B–Ph with the Pd1–Cl1 bond (dihedral angle C1-B1-Pd1-Cl1 of  $10.6(3)^{\circ}$ ). The <sup>31</sup>P NMR spectrum of **9** displayed only a singlet resonance at  $\delta$  = 49.9 ppm which suggests a quick interconversion between the two diastereotopic phosphine donors in solution.

Cationic allyl complex  $[(^{Ph}DPB^{Ph})Pd^{II}(\eta^3-C_3H_5)]SbF_6$  (10) was synthesized by reaction of AgSbF<sub>6</sub> with zwitterionic allyl com-

plex  $[{(o-PPh_2C_6H_4)_2B(OAc)Ph}Pd^{II}(C_3H_5)]$  (4) (Scheme 1) and was isolated in 38% yield by crystallization from CH<sub>2</sub>Cl<sub>2</sub>/hexane. Figure 4 depicts its solid-state structure. The Pd<sup>II</sup> center in complex 10 is located in a trigonal-pyramidal environment in which the borane occupies the pseudo-apical position and the C<sub>3</sub>H<sub>5</sub>-ligand and the two phosphines are located in the trigonal-planar positions. A weak Pd<sup>II</sup>→B interaction is indicated by a Pd,B distance of 2.676(5) Å, which is in line with a minor pyramidalization at the borane center ( $\Sigma B_{\alpha}\!=\!354.7^{\circ}$ ) and a broad  $^{11}$ B NMR resonance at  $\delta\!=\!62$  ppm ( $\omega_{1/2}\!=\!1200\pm100$  Hz). A large Pd,C22 distance of 3.066(6) Å eliminates the possibility of a strong  $\eta^2(B,C) \rightarrow Pd^{\parallel}$  interaction. The  $\eta^3$ -coordinated  $C_3H_5$ ligand is disordered. Using the borane as a reference point, a 39:61 mixture of the exo- and endo-isomers is observed. A wider P-Pd-P angle of 102.86(5)° is realized by a decrease in the twisting of the ligand backbone (dihedral angle C18-C17-C28-C33 of 24.04°). The observed disorder of the C<sub>3</sub>H<sub>5</sub>-ligand is in good agreement with the observed NMR spectra. In the <sup>31</sup>P NMR spectrum (CD<sub>2</sub>Cl<sub>2</sub>), two singlet resonances are observed in a 40:60 ratio ( $\delta$  = 28.1 and 26.9 ppm) and two sets of  $C_3H_5$ -units are detected in the  $^1H$  NMR spectrum. DFT calculations (BP86/def-SV(P)) based on the solid-state structures of 10-endo and 10-exo indicate a small Gibbs free energy preference of  $\Delta G = 0.74 \text{ kcal mol}^{-1}$  for **10-endo**, predicting a 29:71 ratio at 298 K.

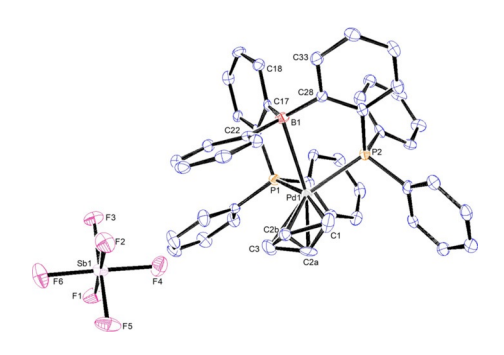


**Figure 4.** Thermal ellipsoid plot of the solid-state structure of **10** at the 50 % probability level. Hydrogen atoms and one molecule of  $CH_2CI_2$  are omitted for clarity. Selected bond lengths (Å) and angles (°): Pd1-B1=2.676(5), Pd1-C22=3.066(6), Pd1-P1=2.304(1), Pd1-P2=2.340(1), Pd1-C1=2.191(5), Pd1-C2a=2.186(12), Pd1-C2b=2.192(7), Pd1-C3=2.201(4), P1-Pd1-P2=102.86(5), P1-Pd1-B1=82.1(1), P2-Pd1-B1=75.1(1). [24]

To explore the potential influence of the  $Pd^{II} \rightarrow B$  interaction on reductive elimination proceeding via an inner-sphere mechanism, complex [( $^{Ph}DPB^{Ph})Pd^{II}(4-NO_2-C_6H_4)I$ ] (5) was reacted with lithium amides. Complex 5 was reacted with LiNMe<sub>2</sub> (1.1 equiv) at room temperature in [D<sub>8</sub>]THF (Scheme 3).<sup>[25]</sup>

A conversion of 84% was observed <sup>31</sup>P NMR spectroscopically after 1 h. Two complexes were formed with singlet resonances at  $\delta$ =31.1 (70%) and 38.3 ppm (14%). After a total of 4.5 h, all resonances in the <sup>31</sup>P NMR spectrum disappeared in favor of the singlet at  $\delta$ =31.1 ppm. <sup>11</sup>B NMR spectroscopy suggested formation of a zero-valent palladium complex by a broad resonance at  $\delta$ =19 ppm ( $\omega_{1/2}$ =400  $\pm$ 100 Hz). The concurrent formation of the expected reductive elimination prod-



Scheme 3. Reductive elimination from 5 and independent synthesis of 11.

uct *N,N*-dimethyl-4-nitroaniline was confirmed by GC/MS analysis, using an independently prepared sample as a reference. The absence of an intermediate complex cis-[( $^{Ph}DPB^{Ph}$ )Pd $^{II}$ (4-NO<sub>2</sub>-C<sub>6</sub>H<sub>4</sub>)NMe<sub>2</sub>] suggests that transmetalation is rate-limiting in this transformation. The intermediate occurrence of the  $^{31}P$  NMR resonance at  $\delta=38.3$  ppm is possibly due to a reversible reaction of LiNMe<sub>2</sub> with complex **6**. In a control experiment complex [( $^{Ph}DPB^{Ph}$ )Pd $^{O}$ (pyridine)] (1) was reacted with LiNCy<sub>2</sub> and LiNMe<sub>2</sub> in [D<sub>8</sub>]THF. In both cases ca. 7% of a new complex at  $\delta=38.5$  (s) and 37.7 ppm (s) were observed.

Complex **6** decomposed within hours with simultaneous precipitation of palladium black. Addition of PMe<sub>3</sub> as a stabilizing co-ligand led to the formation of complex [( $^{Ph}DPB^{Ph}$ )Pd<sup>0</sup>(PMe<sub>3</sub>)] **11**. The  $^{31}P$  NMR spectrum of **11** showed a doublet at  $\delta=35.3$  and a triplet at -40.1 ppm (J=15.1 Hz) in a 2:1 ratio, which is consistent with the expected  $\kappa^3P$ -coordination. The broad resonance in the  $^{11}B$  NMR spectrum at  $\delta=25$  ppm ( $\omega_{1/2}=400\pm100$  Hz) suggested a strong Pd<sup>0</sup> $\rightarrow$ B interaction. Complex **11** could also be synthesized independently by reaction of PBP pincer **12** with PhLi and PMe<sub>3</sub>, or reaction of **1** with PMe<sub>3</sub>, thus confirming unambiguously the identity of **11** (Scheme 3).

Complex **5** reacted in a similar fashion with  $LiNCy_2$  (26% **6** after 3 h) and LiNHtBu (14% **6** after 5.5 h). However, the reaction proceeded slower with these sterically more demanding substrates. The reaction of complex **5** with LiNHtBu was monitored for 96 h by <sup>31</sup>P NMR spectroscopy (46% conversion towards **6**) without any side products being observed (cf. Table S1). This is in line with the assumption of a rate-determining transmetalation followed by a quick reductive elimination.

#### Analyses of Pd→B interactions

The solid-state structures of Pd<sup>0/II</sup> DPB complexes were analyzed to identify factors which affect the strength of Pd→B interactions. In addition to the new Pd complexes presented in this work (6-10), the structurally characterized DPB complexes  $cis-[(^{Ph}DPB^{Ph})Pd^{II}(4-NO_2-C_6H_4)I]$  (5), $^{[9d]}$  [( $^{Ph}DPB^{Ph})Pd^{0}(pyridine)]$  $(1)_{r}^{[3b]}$  [( $^{Ph}DPB^{Me})Pd^{0}(PMe_{3})$ ]  $(13)^{[9d]}$  and [( $^{Cy}DPB^{Ph})Pd^{0}$ ]  $(3)^{[3c]}$ (Figure 4) were included to cover a broad range of B-/P-substituents and co-ligands at the Pd<sup>0/II</sup> center. The shorter Pd,B distances and higher degree of borane pyramidalization (Table 1) confirm a significantly stronger Pd,B interaction in Pd<sup>0</sup> complexes, than in Pd<sup>II</sup> complexes. Surprisingly, within a given oxidation state only a very moderate variation of the  $Pd \rightarrow B$ bond strength is observed, regardless of substituents at the borane and phosphines, or the number and nature of co-ligands (Pd<sup>0</sup>:  $\Sigma B_a = 338-346^\circ$ , d(Pd<sup>0</sup>,B) = 2.194(3) -2.243(2) Å vs.  $Pd^{\parallel}$ :  $\Sigma B_a = 354-356^{\circ}$ ,  $d(Pd^{\parallel},B) = 2.676(5) -2.762(2)$  Å). Remarkably, even the generation of cationic Pd<sup>II</sup> complexes (9 and 10) has no significant impact on the strength of Pd<sup>II</sup>→B interactions. The oxidation state at Pd is unambiguously the dominant factor for the strength of the Pd,B bond.

The  $Pd \rightarrow B$  interactions were further analyzed using QM calculations. Complexes 1, 3, 5–11 and 13 were geometrically optimized using Turbomole 7.0.1 (BP86/def-SV(P)). A good agreement was observed between the optimized structures and their corresponding solid-state structures (Table 1). Complexes 6 and 8 were constructed based on the solid-state

Table 1. Experimental and computational analysis of the $Pd \rightarrow B$ interactions. [a]											
	7	8	9 <sup>[e]</sup>	10-endo	5	1	13	3	6		
d(Pd,B) [Å] (XRD/DFT)	2.762(3)	_	2.721(5)	2.676(5)	2.7402(4)	2.194(3)	2.278(3)	2.243(2)	_		
	2.740	-2.654	2.554	2.731	2.781	2.193	2.360	2.264	-2.253		
$(Pd,C_{ipso})$ [Å] (XRD/DFT)	3.405(3)	_	3.338(4)	3.066(6)	3.346(4)	2.463(3)	2.815(2)	3.079(2)	_		
	3.256	-3.292	3.112	3.259	3.440	2.865	2.685	3.054	-2.768		
$\Sigma B_{\alpha}$ [°] (XRD/DFT)	355/355	-/352	356/355	355/355	354/351	346/346	338/341	341/343	-/349		
$^{11}$ B NMR ( $\delta$ , $\omega_{1/2}$ )	-	-	65 ppm 1900 Hz	67 ppm 1400 Hz	63 ppm 3000 Hz	20 ppm 400 Hz	25 ppm 500 Hz	22 ppm 800 Hz	19 ppm 400 Hz		
$E_2(Pd,B)^{[b]}$ [kcal/mol]	11.46	10.42	11.41	8.04	8.72	23.46	19.53	46.83	42.12		
NLMO %B <sup>[c]</sup> /Pd <sup>[c]</sup>	6.6/91.9	6.3/92.2	5.4/92.9	3.7/93.9	4.7/93.4	16.0/78.7	15.0/81.5	15.5/81.7	14.3/83.0		
occ. B <sup>[d]</sup>	0.391	0.387	0.400	0.360	0.353	0.618	0.621	0.498	0.519		
occ. Pd <sup>[d]</sup>	1.859	1.865	1.870	1.887	1.879	1.666	1.702	1.686	1.704		
B-hybrid % (s/p)	7.6/92.4	7.2/2.7	7.2/92.7	6.7/93.3	6.4/93.6	11.6/88.4	13.9/86.1	12.8/87.2	10.7/89.3		
WBI (Pd,B)	0.2164	0.2063	0.2119	0.1738	0.1801	0.4207	0.3634	0.5032	0.4604		
WBI (Pd,C <sub>ipso</sub> )	0.0079	0.0079	0.0208	0.0093	0.0062	0.0697	0.0171	0.0103	0.0325		

[a] Structure optimization: Turbomole 7.0.1, BP86/def-SV(P); NBO analysis: Gaussian 09/NBO 6.0, BP86/6-31G(d), MWB10 (P,Cl), MWB28 (Pd, Br), MWB46 (I). [b] NBO stabilizing energy  $E_2$  associated with the Pd $\rightarrow$ B interaction. [c] Contribution of the donor/acceptor NBO to the NLMO. [d] Occupancy of the donor/acceptor NBO. [e] Calculated structure parameters of **9** are based on the monomer.



structure of complexes **1** and **7**. The  $Pd \rightarrow B$  interactions were further analyzed using NBO/NLMO calculations. In all cases, an NBO donor/acceptor interaction was found between an occupied d-orbital at Pd and an unoccupied p-orbital at B (Figure 5). For all examined complexes no relevant  $\eta^2(B,C)$ -coordination was found in the NBO calculations. The Wiberg bond index for Pd, $C_{ipso}$  was below 0.02, with the exception of Pd<sup>0</sup> complexes **1** (0.0697) and **6** (0.0325). Reactivity studies of [(DPB)Pd]-complexes presented in this paper thus appear to be unaffected from significant  $\eta^2(B,C)$ -coordination.

The NBO stabilizing energy of this  $Pd \rightarrow B$  interaction varied depending on the Pd oxidation state. For  $Pd^{II} \rightarrow B$  interactions, a narrow range of NBO stabilizing energies between 8.04 and 11.46 kcal mol<sup>-1</sup> was observed. Surprisingly, generation of cationic complexes (**9**, **10-endo**), exchange of chloro-ligands by bromide (**8**) or iodide/aryl (**5**) had very little effect. In the case of  $Pd^{0} \rightarrow B$  interactions, significantly higher NBO stabilizing energies of 19.53–46.83 kcal mol<sup>-1</sup> were found. Regardless of the oxidation state at Pd an approximately linear correlation between the Pd,B distance and the NBO stabilizing energy ( $E_2$ ) associated with the Pd,B interaction was observed (Figure 6) for

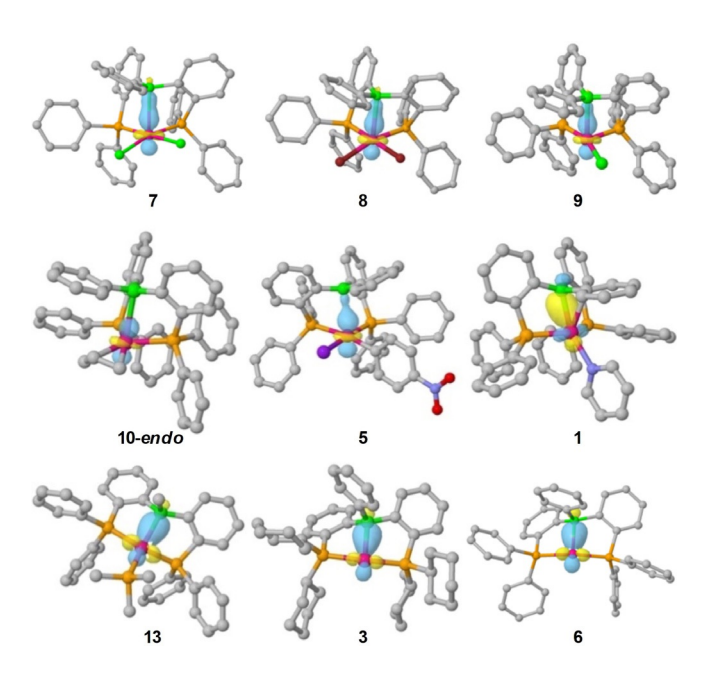


**Figure 5.** Graphical representation of the NLMOs associated with the  $Pd \rightarrow B$  interactions in [ $(P^hDPB^{Ph})Pd(0/II)$ ] complexes.

16 valence electron (VE) complexes 1, 5, 7, 8, 10 and 13. The Pd,B distance appears to be dictated by the Pd,B bond strength, and not by constraints imposed by the chelating ligand. Substitution of PPh<sub>2</sub>-groups (6) by PCy<sub>2</sub>-groups (3) had only a minor effect. The  $E_2$  values for the Pd<sup>0</sup> $\rightarrow$ B interaction in the 14 VE complexes 3 (46.83 kcal mol<sup>-1</sup>) and 6 (42.12 kcal mol<sup>-1</sup>) significantly deviate from this correlation and are almost twice as much as for 16 VE complexes 1 (23.46 kcal mol<sup>-1</sup>) and 13 (19.53 kcal mol<sup>-1</sup>). Neither the <sup>11</sup>B NMR chemical shift, Pd,B distance or pyramidalization at B indicate a change of the Pd<sup>0</sup> $\rightarrow$ B interaction strength in this magnitude between the 14 VE and the 16 VE complexes (Table 1). This discrepancy might be explained by the difficulty to compare the 2<sup>nd</sup> order perturbation interaction energies from NBO analysis from 14 VE with 16 VE complexes.

The <sup>11</sup>B NMR resonances are shifted linearly towards higher field with an increasing Pd,B distance for Pd<sup>0</sup> complexes, regardless of the valence electron count at the Pd center (Figure 6). Complex [(PhDPBPh)Pd<sup>0</sup>(PPh<sub>3</sub>)] (2) reported by Kameo and Bourissou<sup>[3e]</sup> also fits perfectly into this correlation (d(Pd,B) = 2.294(2) Å,  $\delta$ (11B) 27 ppm). In contrast, the <sup>11</sup>B NMR resonance shifts linearly towards lower field with an increasing Pd,B distance in case of Pd<sup>II</sup> complexes. <sup>11</sup>B NMR spectroscopy therefore can be used as a tool to assess the strength of Pd  $\rightarrow$  B interactions within a given ligand system, provided that the oxidation state at the Pd center is taken into account. However, given the difficulty to determine the precise  $\delta$ (11B) of [(DPB)Pd<sup>II</sup>] complexes (poor solubility and  $\omega_{1/2} > 1000$  Hz ), a certain error for weak Pd<sup>II</sup> $\rightarrow$ B interactions needs to be factored in. <sup>[26]</sup>

Quantum chemical calculations (DFT) were used to model the inner-sphere reductive elimination of *N,N*-dimethyl-4-nitro-aniline from complex **14-B** (Scheme 4). C–N bond formation is predicted to proceed via an inner sphere reductive elimination with a low activation barrier of  $\Delta G^{\pm} = +7.90 \text{ kcal mol}^{-1}$  (transition state **15-B**), yielding Pd<sup>0</sup> complex **6** and *N,N*-dimethyl-4-nitroaniline (overall  $\Delta G = -58.75 \text{ kcal mol}^{-1}$ ). In order to understand how the Pd<sup>II</sup>  $\rightarrow$ B interaction affects the reductive elimination, the reaction was also modeled for bis[(2-diphenylphosphino)phenyl]ether (DPEphos) complex **14-O** and diphosphinoamine complex **14-N**. DPEphos is well established as an effective ligand in palladium catalyzed Buchwald–Hartwig-type coupling reactions, [27] and commands very similar structural features to PhDPBPh (Table 2). However, DPEphos cannot mimic

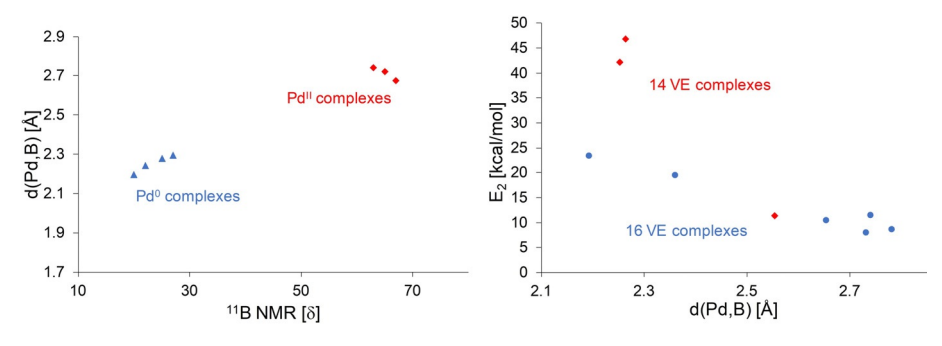


Figure 6. Left: correlation between solid state Pd,B distances and  $\delta(^{11}B)$ . Right: correlation between calculated Pd,B distances and NBO stabilizing energies.



Table 2. Computational analysis of C–N bond formation from complexes 14-B, 14-O and 14-N. <sup>[a]</sup>										
E=B, O, N	14-B	15-B	6	14-0	15-0	16-0	14-N	15-N	16-N	
<i>d</i> (Pd,E) [Å]	2.845	2.947	2.253	3.343	3.349	2.955	3.360	3.381	3.023	
d(C,N) [Å]	2.904	2.084	-	2.816	2.077	_	2.801	2.068	_	
d(Pd,C) [Å]	2.042	2.059	-	2.036	2.051	_	2.033	2.051	_	
d(Pd,N) [Å]	2.102	2.108	-	2.091	2.102	_	2.089	2.100	_	
≰ (P,Pd,P) [°]	101.2	101.0	147.1	100.4	102.0	136.4	97.5	98.8	132.9	
q(Pd) [b]	+0.376	+0.330	+0.055	+0.318	+0.275	-0.162	+0.320	+0.276	-0.123	
q(E) <sup>[b]</sup>	+0.722	+0.735	+0.527	-0.498	-0.496	-0.485	-0.448	-0.448	-0.444	
WBI(Pd,E) <sup>[c]</sup>	0.193	0.162	0.460	0.005	0.005	0.005	0.005	0.005	0.005	
$\Sigma B_{a}$ [°]	355.4	354.6	348.8	-	-	-	-	-	-	

[a] Structure optimization: Turbomole 7.0.1, BP86/def-SV(P); NBO analysis: Gaussian 09/NBO 6.0, BP86/6-31G(d), MWB10 (P), MWB28 (Pd). [b] Natural population analysis (NPA) charge. [c] Wiberg bond index.

Scheme 4. Reductive elimination of *N,N*-dimethyl-4-nitroaniline from PEP complexes 14-B, 14-O and 14-N.

the potential steric effect of the B-Ph group on the coordinated reactive ligands. For this reason, the diphosphinoamine ligand (o-PPh<sub>2</sub>C<sub>6</sub>H<sub>4</sub>)<sub>2</sub>NPh<sup>[28]</sup> has also been included in the theoretical considerations, as its N-Ph bridgehead gives a good model of the B-Ph group in 14-B. Elimination of N,N-dimethyl-4-nitroaniline from complexes 14-O and 14-N gave very similar Gibbs free reaction energies of  $\Delta G = -38.52 \text{ kcal mol}^{-1}$  and  $\Delta G = -38.63 \text{ kcal mol}^{-1}$ , respectively. No Pd<sup>0/II</sup> $\rightarrow$ E interactions were observed in complexes featuring DPEphos and the diphosphinoamine ligand (Table 2, WBI(Pd,E) = 0.005, E = O, N). Given the high structural similarity of complexes 6, 16-0 and **16-N** the increase of  $\Delta G$  by ca. 20 kcal mol<sup>-1</sup> in case of the PhDPBPh ligand is a good approximation for the increase of the  $Pd^0 \rightarrow B$  interaction strength in **6** compared to the  $Pd^{\parallel} \rightarrow B$  interaction strength in complex 14-B. When switching from PhDBPPh to DPEphos, a small decrease of  $\Delta\Delta G^{\dagger} = 0.41 \text{ kcal mol}^{-1}$  was found for the reductive elimination barrier (Scheme 4). This was surprising, as a more facile reductive elimination was expected from 14-B than from 14-O, due to 1) an electronic effect by Pd→B coordination and 2) increased steric bulk of the DPB ligand imposed by the B-Ph group. In case of diphosphinoamine complex 14-N the reductive elimination barrier decreased to  $\Delta G^{\dagger} = 5.54 \text{ kcal mol}^{-1}$  ( $\Delta \Delta G^{\dagger} = 2.46 \text{ kcal mol}^{-1}$ ), possibly as a result of the increased steric pressure imposed by the *N*-Ph group (Table 2). Reductive elimination from **14-E** (E = B, O, N) proceeds via structurally early transition-state 15-E (Figure 7).

Unexpectedly, the Pd $\rightarrow$ B interaction is slightly weakened in transition-state **15-B**, compared to starting complex **14-B**, as indicated by a slightly elongated Pd,B distance (2.947 Å) in **15**-

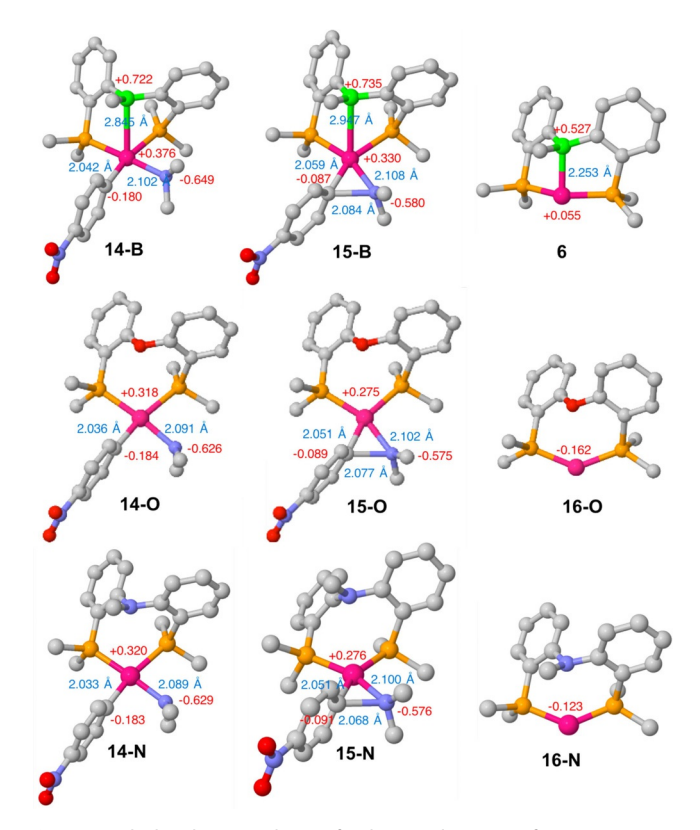


**Figure 7.** Calculated intermediates of reductive elimination from **14-B** (top), **14-O** (middle) and **14-N** (bottom). For clarity the H atoms are omitted, and only the  $C_{ipso}$  atoms of the Ph-groups at B and P are shown. Red: NPA charges, blue: bond distances.

**B** compared to **14-B** (2.906 Å). Similarly, the Wiberg bond index for the  $Pd \rightarrow B$  interaction is reduced to 0.162 in **15-B** (**14-B**: 0.176), and the NPA charge at the borane remains unchanged (**14-B**: +0.737 vs. **15-B**: +0.735). The increase of the  $Pd \rightarrow B$  interaction strength occurs after the reductive elimination, explaining why the inner-sphere reductive elimination of the C-N bond does not kinetically profit from the substantial increase of the  $Pd \rightarrow B$  strength in the course of the reaction.

To rule out effects originating from restraints imposed by a chelating ligand frame work, the reductive elimination of  $N_1$ -dimethyl-4-nitroaniline was also modeled using *cis*-[(PMe<sub>3</sub>)<sub>2</sub>Pd<sup>II</sup>(4-NO<sub>2</sub>C<sub>6</sub>H<sub>4</sub>)NMe<sub>2</sub>] (17,  $\Delta G$  = 37.47 kcal mol<sup>-1</sup>) and its



BH<sub>3</sub> adduct [(PMe<sub>3</sub>)<sub>2</sub>(BH<sub>3</sub>)Pd<sup>II</sup>(4-NO<sub>2</sub>C<sub>6</sub>H<sub>4</sub>)NMe<sub>2</sub>] (**17-B**,  $\Delta G$  = 49.19 kcal mol<sup>-1</sup>) as substrates (cf. Scheme S1). Again, a more favorable transition state was found for the acceptor free complex **17** ( $\Delta G$ <sup>+</sup> = +7.35 kcal mol<sup>-1</sup>), than for the borane adduct **17-B** ( $\Delta G$ <sup>+</sup> = +8.55 kcal mol<sup>-1</sup>).

# **Conclusions**

The strength of  $Pd \rightarrow B$  interactions in [(DPB)Pd] complexes depends primarily on the oxidation state of Pd. In contrast, modifications of the DPB ligand or co-ligands have only a minor effect. <sup>11</sup>B NMR spectroscopy has been established as a useful tool to assess the strength of  $Pd \rightarrow B$  interactions in solution. Reaction of lithium amides with  $[(P^hDPB^{Ph})Pd^{II}(4-NO_2C_6H_4)I]$  (5) chemoselectively yields the C-N coupling product and  $[(P^hDPB^{Ph})Pd^{II}]$  (6). Inner-sphere reductive C—N bond elimination was modelled with DFT methods for the  $P^hDPB^{Ph}$  ligand. In contrast to reports on acceptor promoted outer-sphere reductive C—N bond elimination, <sup>[5b, 17]</sup> no significant effect of the borane acceptor on the inner-sphere reductive elimination rate was found. This is explained by the fact that the strengthening of the  $Pd \rightarrow B$  bond occurs after the reductive elimination.

# **Experimental Section**

#### General

All manipulations were performed under an argon atmosphere using standard Schlenk line and glovebox techniques. Glassware was oven dried at  $120\,^{\circ}\text{C}$  overnight and dried with a heat gun under vacuum prior to use. Tetrahydrofuran was dried by an MBraun solvent purification system. Benzene and n-hexane were dried over sodium, distilled under argon prior to use and stored over activated molecular sieves (4 Å).

 $\text{CD}_2\text{Cl}_2$  and  $\text{C}_6\text{D}_6$  were degassed employing the freeze-pump-thaw technique and stored over activated molecular sieves (4 Å). [D\_8]THF was dried over activated molecular sieves (3 Å), distilled under an argon atmosphere and degassed employing the freeze-pump-thaw technique.  $^{\text{Ph}}\text{DPB}^{\text{Ph}}$ , [( $^{\text{Ph}}\text{DPB}^{\text{Ph}}\text{OAc}$ )Pd(C\_3H\_5)] (4), [( $^{\text{Ph}}\text{DPB}^{\text{Ph}}$ )Pd(4-NO\_2C\_6H\_4)I] (5) and [{(o-PPh\_2C\_6H\_4)\_2BPh}PdI] (12) were synthesized according to published procedures. [3b,9d]

NMR-experiments were performed in Wilmad® quick pressure valve NMR tubes. ¹H, ¹¹B{¹H}, ¹³C{¹H}, ¹°F{¹H}, and ³¹P{¹H} NMR spectra were recorded on a Bruker Avance II (400.1 MHz, probe: BBO) or a Bruker Avance (400.3 MHz, probe: ATM BBFO) spectrometer. ¹H and ¹³C{¹H} NMR spectra were referenced to residual solvent resonances as implemented in MesReNova 10.0.2. Infrared spectra were recorded on an Avatar 360 FT-IR E.S.P. device by Nicolet. CHN combustion analysis were carried out on an Elementar EL device by Elementar Analysesysteme GmbH.

Deposition Number(s) 1987620 (7), 1987625 (9) and 1987626 (10) contain(s) the supplementary crystallographic data for this paper. These data are provided free of charge by the joint Cambridge Crystallographic Data Centre and Fachinformationszentrum Karlsruhe Access Structures service www.ccdc.cam.ac.uk/structures.

#### **Reactivity studies**

A solution of the respective lithium amide (5.7  $\mu$ mol, 1.1 equiv) in [D<sub>8</sub>]THF (0.25 mL) was added dropwise over a period of 4 min to a

stirred solution of nitroarene complex **5** (5.0 mg, 5.2  $\mu$ mol, 1.0 equiv) in [D<sub>8</sub>]THF (0.25 mL). The resulting mixture was stirred for another 5 min and then transferred into an NMR tube. Reductive elimination was monitored by <sup>31</sup>P NMR spectroscopy.

# Synthesis of [(PhDPBPh)PdCl<sub>2</sub>] (7)

CH<sub>2</sub>Cl<sub>2</sub> (8 mL) was added to a mixture of PhDPBPh (400 mg, 0.665 mmol, 1.0 equiv) and [(cod)PdCl<sub>2</sub>] (187 mg, 0.665 mmol, 1.0 equiv). The mixture was stirred for 30 min at room temperature. Yellow crystals (380 mg, 0.482 mmol, 74%) were formed by overlaying the solution *n*-pentane (16 mL). Single crystals suitable for X-ray diffraction were grown from a solution of [(cod)PdCl<sub>2</sub>] (9.7 mg, 34  $\mu mol,$  1.0 equiv) and  $^{Ph}DPB^{Ph}$  (21.2 mg, 34.7  $\mu mol,$ 1.0 equiv) in CD<sub>2</sub>Cl<sub>2</sub> (0.7 mL) overlaid with benzene (0.3 mL). <sup>11</sup>B and <sup>13</sup>C NMR data have not been collected due to poor solubility.  $^{1}$ H NMR (400.13 MHz, CD<sub>2</sub>Cl<sub>2</sub>, 25  $^{\circ}$ C):  $\delta$  7.81–7.76 (m, 2 H), 7.55 (tdd, J=7.3, 3.0, 1.1 Hz, 3 H), 7.50-7.46 (m, 3 H), 7.46-7.38 (m, 6 H), 7.35-7.14 (m, 13 H), 6.97–6.78 (m, 5 H), 5.32 (s, 2 H,  $CH_2CI_2$ ).  $^{31}P\{^{1}H\}$  NMR (161.98 MHz, CD<sub>2</sub>Cl<sub>2</sub>, 26 °C):  $\delta$  44.5 (s,  $w_{1/2}$ =570 Hz). IR (KBr):  $\tilde{\nu}$ = 3643-3284 (w), 3049 (w), 1587 (w), 1497 (m), 1433 (vs., sh), 1223 (s), 1158 (vw), 1128 (w), 1093 (vs.), 987 (w), 889 (vw), 864 (vw), 754 (s), 744 (s), 733 (m), 688 (vs.), 667 (w), 611 (m), 600 (s), 542 (m), 523 (vs.), 505 (m) cm<sup>-1</sup>. Elemental analysis calcd (%) for C<sub>42</sub>H<sub>33</sub>BCl<sub>2</sub>P<sub>2</sub>Pd·CH<sub>2</sub>Cl<sub>2</sub>: C 59.18, H 4.04, found: C 59.61, H 4.33.

# Synthesis of [(PhDPBPh)PdBr2] (8)

The  $^{\rm Ph}{\rm DPB}^{\rm Ph}$  ligand (200 mg, 0.328 mmol, 1.0 equiv) and [(cod)PdBr<sub>2</sub>] (122.7 mg, 0.328 mmol, 1.0 equiv) were solved in DCM (10 mL) and stirred at r.t. for 30 min. The solution was overlaid with n-hexane (20 mL) yielding title compound **8** as orange crystals (192.0 mg, 0.219 mmol, 67 %).  $^{11}{\rm B}$  and  $^{13}{\rm C}$  NMR data have not been collected due to poor solubility.  $^{1}{\rm H}$  NMR (400.30 MHz, CD<sub>2</sub>Cl<sub>2</sub>):  $\delta$  7.85–7.76 (m, 3 H), 7.59–7.19 (m, 30 H).  $^{31}{\rm P}\{^{1}{\rm H}\}$  NMR (162.04 MHz, CD<sub>2</sub>Cl<sub>2</sub>):  $\delta$  45.2 (bs, 1P, w<sub>1/2</sub>=450 Hz), 38.1 (bs, 1P, w<sub>1/2</sub>=450 Hz). IR (KBr):  $\bar{\nu}$  = 3424 (s), 3048 (m), 1621 (w), 1587 (w), 1478 (m), 1455 (w), 1432 (s), 1311 (w), 1237 (w), 1220 (s), 1205 (m), 1187 (m), 1153 (w), 1126 (m), 1092 (s), 1027 (w), 1000 (m), 887 (w), 863 (w), 753 (s), 741 (s), 713 (m), 699 (s), 690 (s), 667 (m), 610 (s), 600 (s), 539 (s), 522 (s), 505 (s), 465 (m) cm $^{-1}$ . Elemental analysis calcd (%) for C<sub>42</sub>H<sub>33</sub>BBr<sub>2</sub>P<sub>2</sub>Pd·0.25CH<sub>2</sub>Cl<sub>2</sub>: C 56.51; H 3.76, found: C 56.72, H 3.83.

# Synthesis of [(PhDPBPh)PdCl]SbF<sub>6</sub> (9)

Complex 7 (200 mg, 254  $\mu$ mol, 1.0 equiv) and AgSbF<sub>6</sub> (87.2 mg, 254  $\mu$ mol, 1.0 equiv) were stirred in DCM (15 mL) for 40 minutes. The suspension was filtered through a syringe filter (0.2 μm, PTFE membrane). The clear solution was overlaid with n-hexane (30 mL) yielding the title compound 9 as long colorless needles (128 mg 130 μmol, 51%). <sup>1</sup>H NMR (400.30 MHz, CD<sub>2</sub>Cl<sub>2</sub>):  $\delta$  7.97–7.92 (m, 2 H), 7.80 (tdd, J=7.5, 2.8, 0.9 Hz, 2H), 7.69 (dd, J=7.6, 2.6 Hz, 2H), 7.65 (t, J = 7.5 Hz, 2H), 7.55 (tt, J = 7.4, 1.4 Hz, 1H), 7.47–7.34 (m, 6H), 7.27–7.16 (m, 10 H), 7.00 (dt, J=7.6, 2.4 Hz, 4 H), 6.83 (dd, J=12.4, 7.9 Hz, 4H). <sup>11</sup>B{<sup>1</sup>H} NMR (128.43 MHz, CD<sub>2</sub>Cl<sub>2</sub>):  $\delta$  = 65 (bs, w<sub>1/2</sub> = 1900  $\pm$  300 Hz). <sup>13</sup>C{<sup>1</sup>H} NMR (100.67 MHz, CD<sub>2</sub>Cl<sub>2</sub>):  $\delta = \delta$  141.79, 135.43 (d, J=8.5 Hz), 134.88 (d, J=11.1 -Hz), 134.25, 133.69 (d, J= 19.5 Hz), 133.22 (d, J = 17.4 Hz), 132.49 (d, J = 3.7 Hz), 129.67 (d, J =8.9 Hz), 129.33–128.82 (m), 128.10, 127.13, 126.74, 126.16. <sup>31</sup>P{<sup>1</sup>H} NMR (162.04 MHz, CD<sub>2</sub>Cl<sub>2</sub>):  $\delta$  49.9 (s,  $w_{1/2} = 30$  Hz). IR (KBr):  $\tilde{v} = 3441$ (s), 3058 (w), 1588 (w), 1482 (w), 1435 (s), 1230 (m), 1200 (w), 1125 (w), 1034 (m), 1001 (w), 867 (vw), 752 (s), 702 (s), 692 (s), 659 (vs.), 614 (m), 538 (s), 517 (s), 697 (w) cm<sup>-1</sup>. Elemental analysis calcd (%)



for  $C_{42}H_{33}BCIF_6P_2PdSb\cdot 0.25$   $C_6H_{14}$ : C 51.75, H 3.64, found: C 51.77, H 3.785.

# Synthesis of [(PhDPBPh)Pd(C3H5)]SbF6 (10)

Allyl complex 4 (120 mg, 143 μmol, 1.0 equiv) and AgSbF<sub>6</sub> (49.0 mg, 143  $\mu$ mol, 1.0 equiv) were solved in CH<sub>2</sub>Cl<sub>2</sub> (7 mL) and stirred at r.t. for 20 min. The suspension was filtered through a syringe filter (0.2 μm, PTFE membrane). The clear solution was overlaid with n-hexane (10 mL). The obtained crystals showed insufficient purity and were crystallized again under the same conditions yielding 10 as slightly yellow crystals (50.2 mg, 53.8 μmol, 38%). <sup>1</sup>H NMR (400.30 MHz, CD<sub>2</sub>Cl<sub>2</sub>):  $\delta$  7.72–7.59 (m, 4H), 7.58–7.53 (m, 2H), 7.53-7.44 (m, 13H), 7.43-7.29 (m, 6H), 7.23-7.15 (m, 2H), 7.05-6.87 (m, 5.5 H), 6.78-6.67 (bs, 2 H), 5.88-5.70 (bs, 0.7 H), 3.77-3.61 (bs, 1.3 H), 3.59-3.33 (bs, 1.3 H), 3.03-2.85 (bs, 0.9 H), 2.49-2.29 (bs, 1.2H) (fractional integrals are a result from signal splitting caused by a dynamic process).  $^{11}B\{^1H\}$  NMR (128.38 MHz, CD<sub>2</sub>Cl<sub>2</sub>):  $\delta$ 64 (bs,  $w_{1/2}\!=\!1550\!\pm\!50$  Hz).  $^{13}\text{C}\{^1\text{H}\}$  NMR (100.67 MHz, CD<sub>2</sub>Cl<sub>2</sub>):  $\delta$ 141.1, 140.2, 136.1, 135.5, 135.3, 135.0, 134.4, 134.3, 134.0, 133.2 (t, J=5.8 Hz), 132.3, 132.2, 132.1, 131.6, 131.5, 131.2, 131.0, 129.6 (t, J=5.3 Hz), 129.3, 128.9, 123.1, 80.4, 80.2.  $^{31}P\{^{1}H\}$  NMR (162.04 MHz,  $CD_2CI_2$ ):  $\delta$  28.1 (s, 0.6P), 26.9 (s, 0.4P). IR (KBr):  $\tilde{v} = 3430$  (s), 3000 (m), 1588 (m), 1480 (m), 1458 (w), 1434 (s), 1268 (m), 1227 (s), 1127 (m), 1095 (m), 1031 (w), 999 (w), 950 (vw), 875 (w), 772 (w), 754 (m), 742 (m), 733 (m), 695 (s), 659 (vs.), 609 (s), 537 (m), 521 (s), 478 (w), 430 (w) cm<sup>-1</sup>. Elemental analysis calcd (%) for C<sub>46</sub>H<sub>40</sub>BCl<sub>2</sub>F<sub>6</sub>P<sub>2</sub>PdSb: C 51.22, H 3.74, found: C 51.04, H, 3.86.

# Synthesis of [(PhDPBPh)Pd] (6)

A solution of LiNMe $_2$ ·THF (0.7 mg, 6  $\mu$ mol, 1.1 equiv) in [D $_8$ ]THF (0.25 mL) was added over a period of 3 min to a solution of complex **5** (5.0 mg, 5  $\mu$ mol, 1 equiv) in [D $_8$ ]THF (0.25 mL). The combined solutions were transferred to an NMR tube and NMR spectra were recorded after 1.5 and 4.5 h.  $^{11}$ B{ $^1$ H} NMR (128.38 MHz, [D $_8$ ]THF):  $\delta$  19 (bs, w $_{1/2}$ =550 Hz  $\pm$  50 Hz).  $^{31}$ P{ $^1$ H} NMR (162.04 MHz, [D $_8$ ]THF):  $\delta$  30.93 (s).

# Synthesis of [(PhDPBPh)Pd(PMe3)] (11)

A solution of PhLi (3.2 mg, 38  $\mu$ mol, 1.2 equiv) in THF (0.5 mL) was slowly added to a solution of complex 12 (25 mg, 33 µmol, 1.0 equiv) in THF (0.5 mL). After stirring for 10 min at r.t. a solution of PMe $_3$  in toluene (1.0 M, 50  $\mu$ L, 50  $\mu$ mol, 1.5 equiv) was added. The precipitate was removed by filtration and the solution was concentrated in vacuo. The resulting solid was washed with pentane and dried in vacuo (20.7 mg, 26.1 µmol, 79%). <sup>1</sup>H NMR (400.13 MHz,  $C_6D_6$ ):  $\delta$  8.34 (d, 2H, J=7.8 Hz), 7.69–7.58 (m, 4H), 7.44–7.37 (m, 2H), 7.36–7.28 (m, 4H, Ar-H), 7.12 (t, 2H, J=6.7 Hz), 7.09–7.05 (m, 13 H), 6.85 (m, 2 H), 6.68 (pt, 4 H, J = 7.8 Hz), 0.64 (d,  $^2J_{\text{P-H}}\!=\!5.0~\text{Hz},~9~\text{H},~\text{PMe}_3\text{)}.~^{11}\text{B}\{^1\text{H}\}~\text{NMR}$  (128.38 MHz,  $\text{C}_6\text{D}_6\text{)}:~\delta~25$  (bs,  $W_{1/2} = 740 \text{ Hz } \pm 50 \text{ Hz}$ ). <sup>13</sup>C{<sup>1</sup>H} NMR (100.62 MHz, C<sub>6</sub>D<sub>6</sub>):  $\delta$  168.7 (bs), 143.2 (d, J = 16.3 Hz), 143.0 (d, J = 16.3 Hz), 141.5 (td, J = 15.2, 2.0 Hz), 138.9 (t, J=13.5 Hz), 135.8 (t, J=6.4 Hz), 135.7 (t, J=6.4 Hz) 2.7 Hz), 133.5 (t, J=7.7 Hz), 133.0 (dt, J=16.7, 5.0 Hz), 132.3 (s), 132.3 (s), 132.4 (t, J = 6.7 Hz), 129.5 (s), 129.0 (s), 128.6 (s), 127.2 (s), 126.1 (t, J = 2.8 Hz), 125.2 (s), 18.1 (dt, J = 11.8, 2.2 Hz, PMe<sub>3</sub>).  ${}^{31}P{}^{1}H{}$ NMR (162.04 MHz,  $C_6D_6$ ):  $\delta$  35.44 (d,  ${}^2J_{P-P}=14.1$  Hz, 2P, ArPPh<sub>2</sub>), -40.13 (t,  ${}^{2}J_{P-P} = 14.2$  Hz, 1P, PMe<sub>3</sub>).

# Acknowledgements

We are grateful for the financial support granted by the Funds of the Chemical Industry (fellowship to MET). Simulations were performed with computing resources granted by RWTH Aachen University under project rwth0245. We thank Dr. F. Pan, Dr. C. Merkens and J. Kollath for collection of X-ray diffraction data and Prof. Dr. F. Schoenebeck for kindly providing access to GC/MS analysis. Open access funding enabled and organized by Projekt DEAL.

# **Conflict of interest**

The authors declare no conflict of interest.

**Keywords:** boranes  $\cdot$  donor–acceptor systems  $\cdot$  palladium  $\cdot$  phosphine ligands  $\cdot$  reductive elimination

- a) I. Kuzu, I. Krummenacher, J. Meyer, F. Armbruster, F. Breher, *Dalton Trans.* 2008, 5836–5865; b) F.-G. Fontaine, J. Boudreau, M.-H. Thibault, *Eur. J. Inorg. Chem.* 2008, 5439–5454; c) H. Braunschweig, R. D. Dewhurst, *Dalton Trans.* 2011, 40, 549–558; d) H. Braunschweig, R. D. Dewhurst, A. Schneider, *Chem. Rev.* 2010, 110, 3924–3957; e) A. Amgoune, D. Bourissou, *Chem. Commun.* 2011, 47, 859–871; f) H. Kameo, H. Nakazawa, *Chem. Asian J.* 2013, 8, 1720–1734; g) J. S. Jones, F. P. Gabbaï, *Acc. Chem. Res.* 2016, 49, 857–867; h) G. Bouhadir, D. Bourissou, *Chem. Soc. Rev.* 2016, 45, 1065–1079.
- a) M. Sircoglou, S. Bontemps, G. Bouhadir, N. Saffon, K. Miqueu, W. Gu, M. Mercy, C.-H. Chen, B. M. Foxman, L. Maron, O. V. Ozerov, D. Bourissou, J. Am. Chem. Soc. 2008, 130, 16729-16738; b) M. Sircoglou, S. Bontemps, M. Mercy, N. Saffon, M. Takahashi, G. Bouhadir, L. Maron, D. Bourissou, Angew. Chem. Int. Ed. 2007, 46, 8583-8586; Angew. Chem. 2007, 119, 8737-8740; c) M. Garçon, C. Bakewell, G. A. Sackman, A. J. P. White, R. I. Cooper, A. J. Edwards, M. R. Crimmin, Nature 2019, 574, 390-393; d) M. E. Tauchert, J. Okuda, Angew. Chem. Int. Ed. 2020, 59, 4214-4215; Angew. Chem. 2020, 132, 4242-4243.
- [3] a) W. H. Harman, J. C. Peters, J. Am. Chem. Soc. 2012, 134, 5080-5082;
  b) T. Schindler, M. Lux, M. Peters, L. T. Scharf, H. Osseili, L. Maron, M. E. Tauchert, Organometallics 2015, 34, 1978-1984;
  c) P. Steinhoff, M. E. Tauchert, Beilstein J. Org. Chem. 2016, 12, 1573-1576;
  d) P. Steinhoff, M. Paul, J. P. Schroers, M. E. Tauchert, Dalton Trans. 2019, 48, 1017-1022;
  e) H. Kameo, J. Yamamoto, A. Asada, H. Nakazawa, H. Matsuzaka, D. Bourissou, Angew. Chem. Int. Ed. 2019, 58, 18783-18787; Angew. Chem. 2019, 131, 18959-18963.
- [4] a) M.-E. Moret, J. C. Peters, Angew. Chem. Int. Ed. 2011, 50, 2063 2067; Angew. Chem. 2011, 123, 2111 2115; b) H. Kameo, Y. Hashimoto, H. Nakazawa, Organometallics 2012, 31, 3155 3162; c) D. L. M. Suess, J. C. Peters, J. Am. Chem. Soc. 2013, 135, 12580 12583; d) M.-E. Moret, L. Zhang, J. C. Peters, J. Am. Chem. Soc. 2013, 135, 3792 3795; e) T. J. Del Castillo, N. B. Thompson, D. L. M. Suess, G. Ung, J. C. Peters, Inorg. Chem. 2015, 54, 9256 9262; f) M. V. Vollmer, J. Xie, C. C. Lu, J. Am. Chem. Soc. 2017, 139, 6570 6573; g) M. V. Vollmer, J. Xie, R. C. Cammarota, V. G. Young, Jr., E. Bill, L. Gagliardi, C. C. Lu, Angew. Chem. Int. Ed. 2018, 57, 7815 7819; Angew. Chem. 2018, 130, 7941 7945.
- [5] a) C. M. Conifer, D. J. Law, G. J. Sunley, A. J. P. White, G. J. P. Britovsek, Organometallics 2011, 30, 4060–4066; b) W. K. Walker, B. M. Kay, S. A. Michaelis, D. L. Anderson, S. J. Smith, D. H. Ess, D. J. Michaelis, J. Am. Chem. Soc. 2015, 137, 7371–7378.
- [6] a) H. Fong, M.-E. Moret, Y. Lee, J. C. Peters, Organometallics 2013, 32, 3053-3062; b) W. H. Harman, T.-P. Lin, J. C. Peters, Angew. Chem. Int. Ed. 2014, 53, 1081-1086; Angew. Chem. 2014, 126, 1099-1104; c) S. N. MacMillan, W. Hill Harman, J. C. Peters, Chem. Sci. 2014, 5, 590-597; d) B. R. Barnett, C. E. Moore, A. L. Rheingold, J. S. Figueroa, J. Am. Chem. Soc. 2014, 136, 10262-10265; e) M. Devillard, R. Declercq, E. Nicolas, A. W. Ehlers, J. Backs, N. Saffon-Merceron, G. Bouhadir, J. C. Slootweg, W.



- Uhl, D. Bourissou, *J. Am. Chem. Soc.* **2016**, *138*, 4917–4926; f) Y. Li, C. Hou, J. Jiang, Z. Zhang, C. Zhao, A. J. Page, Z. Ke, *ACS Catal.* **2016**, *6*, 1665
- [7] a) G. R. Owen, Chem. Soc. Rev. 2012, 41, 3535-3546; b) G. R. Owen, Chem. Commun. 2016, 52, 10712-10726; c) A. Maity, T. S. Teets, Chem. Rev. 2016, 116, 8873-8911; d) W.-C. Shih, O. V. Ozerov, Organometallics 2017, 36, 228-233; e) R. C. da Costa, B. W. Rawe, A. lannetelli, G. J. Tizzard, S. J. Coles, A. J. Guwy, G. R. Owen, Inorg. Chem. 2019, 58, 359-367.
- [8] a) J. S. Figueroa, J. G. Melnick, G. Parkin, *Inorg. Chem.* 2006, 45, 7056–7058; b) M. Devillard, E. Nicolas, C. Appelt, J. Backs, S. Mallet-Ladeira, G. Bouhadir, J. C. Slootweg, W. Uhl, D. Bourissou, *Chem. Commun.* 2014, 50, 14805–14808; c) J. S. Jones, F. P. Gabbai, *Chem. Eur. J.* 2017, 23, 1136–1144; d) D. You, H. Yang, S. Sen, F. P. Gabba, *J. Am. Chem. Soc.* 2018, 140, 9644–9651; e) Y. Cao, W.-C. Shih, N. Bhuvanesh, O. V. Ozerov, *Dalton Trans.* 2019, 48, 9959–9961.
- [9] a) F.-G. Fontaine, D. Zargarian, J. Am. Chem. Soc. 2004, 126, 8786–8794;
  b) B. E. Cowie, D. J. H. Emslie, Chem. Eur. J. 2014, 20, 16899–16912;
  c) B. E. Cowie, D. J. H. Emslie, Organometallics 2015, 34, 2737–2746;
  d) D. Schuhknecht, F. Ritter, M. E. Tauchert, Chem. Commun. 2016, 52, 11823–11826;
  e) W.-C. Shih, W. Gu, M. C. MacInnis, S. D. Timpa, N. Bhuvanesh, J. Zhou, O. V. Ozerov, J. Am. Chem. Soc. 2016, 138, 2086–2089;
  f) W.-C. Shih, O. V. Ozerov, J. Am. Chem. Soc. 2017, 139, 17297–17300.
- [10] a) S. Bontemps, M. Sircoglou, G. Bouhadir, H. Puschmann, J. A. K. Howard, P. W. Dyer, K. Miqueu, D. Bourissou, *Chem. Eur. J.* 2008, 14, 731–740; b) P. Steinhoff, R. Steinbock, A. Friedrich, B. G. Schieweck, C. Cremer, K.-N. Truong, M. E. Tauchert, *Dalton Trans.* 2018, 47, 10439–10442.
- [11] R. C. Cammarota, M. V. Vollmer, J. Xie, J. Ye, J. C. Linehan, S. A. Burgess, A. M. Appel, L. Gagliardi, C. C. Lu, J. Am. Chem. Soc. 2017, 139, 14244– 14250.
- [12] J. Takaya, N. Iwasawa, J. Am. Chem. Soc. 2017, 139, 6074-6077.
- [13] a) F. Inagaki, K. Nakazawa, K. Maeda, T. Koseki, C. Mukai, Organometallics 2017, 36, 3005 – 3008; b) F. Inagaki, C. Matsumoto, Y. Okada, N. Maruyama, C. Mukai, Angew. Chem. Int. Ed. 2015, 54, 818 – 822; Angew. Chem. 2015, 127, 832 – 836; c) M. R. Talley, R. W. Stokes, W. K. Walker, D. J. Michaelis, Dalton Trans. 2016, 45, 9770 – 9773.
- [14] a) S. Sen, I.-S. Ke, F. P. Gabbaï, Organometallics 2017, 36, 4224–4230;
   b) H. Yang, F. P. Gabbaï, J. Am. Chem. Soc. 2015, 137, 13425–13432.
- [15] a) H. Tsutsumi, Y. Sunada, Y. Shiota, K. Yoshizawa, H. Nagashima, Organometallics 2009, 28, 1988 – 1991; b) H. Nagashima, T. Sue, T. Oda, A. Kanemitsu, T. Matsumoto, Y. Motoyama, Y. Sunada, Organometallics 2006, 25, 1987 – 1994.
- [16] W. K. Walker, D. L. Anderson, R. W. Stokes, S. J. Smith, D. J. Michaelis, Org. Lett. 2015, 17, 752–755.
- [17] R. W. Carlsen, D. H. Ess, *Dalton Trans.* **2016**, *45*, 9835 9840.

- [18] a) O. Kuhn, H. Mayr, Angew. Chem. Int. Ed. 1999, 38, 343–346; Angew. Chem. 1999, 111, 356–358; b) A. L. Casalnuovo, T. V. RajanBabu, T. A. Avers, T. H. Warren, J. Am. Chem. Soc. 1994, 116, 9869–9882.
- [19] A. Bondi, J. Phys. Chem. 1964, 68, 441-451.
- [20] B. Cordero, V. Gómez, A. E. Platero-Prats, M. Revés, J. Echeverría, E. Cremades, F. Barragán, S. Alvarez, *Dalton Trans.* 2008, 2832–2938.
- [21] S. Bontemps, G. Bouhadir, P. W. Dyer, K. Miqueu, D. Bourissou, *Inorg. Chem.* 2007, 46, 5149–5151.
- [22] Crystal data for **7**:  $C_{42}H_{33}BCl_2P_2Pd$ , M=787.73, triclinic, space group P-1, a=10.3478(8), b=10.9350(8), c=17.6683(13) Å,  $\alpha=77.1150(10)^\circ$ ,  $\beta=76.6190(10)^\circ$ ,  $\gamma=63.6820(10)^\circ$ , V=1726.7(2) ų, Z=2, T=100(2) K,  $\mu$ ( $MoK_{\alpha}$ )=0.816 mm $^{-1}$ , 20998/7120 collected/ unique reflections, R1=0.0367, wR2=0.0851, GOF=1.039.
- [23] Crystal data for **9**:  $C_{86}H_{70}B_2CI_6F_{12}P_4Pd_2Sb_2$ , M=2145.92, triclinic, space group P-1, a=12.236(2) Å, b=13.207(3) Å, c=13.749(3) Å,  $\alpha=79.74(3)^\circ$ ,  $\beta=72.99(3)^\circ$ ,  $\gamma=74.83(3)^\circ$ , V=2038.3(8) ų, Z=1, T=100(2) K,  $\mu(\text{MoK}_{\alpha})=1.439$  mm $^{-1}$ , 15975/8020 collected/ unique reflections, R1=0.0371, wR2=0.0870, GOF=0.922.
- [24] Crystal data for **10**: C<sub>46</sub>H<sub>40</sub>BCl<sub>2</sub>F<sub>6</sub>P<sub>2</sub>PdSb, M=1078.58, monoclinic space group, P21/c, a=12.059(2) Å, b=18.635(2) Å, c=19.780(2) Å,  $\beta$ =107.340(2)°, V=4242.8(8) ų, Z=4, T=100(2) K,  $\mu$ (MoK $_{\alpha}$ )=1.322 mm $^{-1}$ , 51175/8800 collected/ unique reflections, R1=0.0412, wR2=0.0837, GOF=1.008.
- [25] The activated 4-NO<sub>2</sub>-C<sub>6</sub>H<sub>4</sub> group was chosen, as previous studies demonstrated that introduction of Pd-Ar groups such as Ph, 4-OMe-C<sub>6</sub>H<sub>4</sub> or 4-CF<sub>3</sub>-C<sub>6</sub>H<sub>4</sub> will result in a cascade of reactions eventually leading to the formation of [(o-PPh<sub>2</sub>-C<sub>6</sub>H<sub>4</sub>)<sub>2</sub>BPdI] (cf. ref. 9d). In a control experiment LiNMe<sub>2</sub> was reacted with 1-iodo-4-nitrobenzene in THF, resulting in an unselective product mixture.
- [26] For Ru boratrane complexes only a poor correlation betweend Ru,B distance and <sup>11</sup>B NMR chemical shift has been observed, see: M. R. S. J. Foreman, A. F. Hill, C. Ma, N. Tshabang, A. J. P. White, *Dalton Trans.* 2019, 48. 209 219.
- [27] a) M. S. Driver, J. F. Hartwig, J. Am. Chem. Soc. 1997, 119, 8232–8245;
   b) B. J. Margolis, K. A. Long, D. L. T. Laird, J. C. Ruble, S. R. Pulley, J. Org. Chem. 2007, 72, 2232–2235.
- [28] J. H. Pawlow, T. E. Hogan, US 2010/0093920A1 (Bridgestone America), USA, 2010.

Manuscript received: March 8, 2020 Revised manuscript received: April 20, 2020 Accepted manuscript online: May 19, 2020 Version of record online: September 18, 2020

www.chemeuri.org